

Nanogold-based photosensitizers probes for dual-model bioimaging and therapy of cancer

Jennifer M Connolly¹, Vijay Raghavan¹, Peter Owens², Antony Wheatley³, Ivan Keogh⁴, Peter Dockery² and Malini Olivo^{1*}

¹School of Physics, National University of Ireland, Galway, University Road, Galway, Ireland

²Anatomy, National University of Ireland Galway, University Road, Galway, Ireland

³Physiology, National University of Ireland Galway, University Road, Galway, Ireland

⁴Consultant Otolaryngologist, Head & Neck Surgeon, Academic Department of Otorhinolaryngology, National University of Ireland Galway and Galway University Hospital, Ireland

Abstract

Reported here is the use of novel nanogold based photosensitizers (nanosensitizers) as optical diagnostic probes and as potential photodynamic and photothermal cancer therapeutic agents using an *in vitro* cancer cell model. Such multimodal nanosensitizers were constructed by layering photosensitizers (Hypericin, Chlorin e6) onto multi-branched gold nanoparticles. Nanosensitizers were conjugated to tumour-specific antibodies to confer cancer-cell specificity. Both oral (SCC9) and breast cancer (MCF7) cell lines were cultured *in vitro* with various concentrations of nanosensitizers. Cellular uptake and intracellular localisation of nanosensitizers was assessed using darkfield contrast imaging, transmission electron microscopy and Raman spectroscopy imaging and quantified using confocal fluorescence microscopy. In addition to photodynamic diagnosis (PDD) efficacy, the photodynamic (PDT) and photothermal (PTT) therapeutic potential of these novel nanosensitizers was assessed. Treated cells were exposed to light of appropriate wavelength and fluence, and cytotoxicity was examined using the 3-(4,5-dimethylthiazol-2-yl)-2,5-diphenyl tetrazolium bromide (MTT) assay. It was observed that nanosensitizers were taken up by cells and internalized. While the intracellular target of nanosensitizers appeared to be cell type-dependent, they were found to localise preferentially to lysosomes and mitochondria. The nanosensitizers were shown to exert minimal dark toxicity, and significant photodynamic-mediated cell death was observed in the micromolar concentration range ($p < 0.05$). Results from this study suggest a cell-type and photosensitizer-type dependence on the rate of nanosensitizer cellular uptake and intracellular distribution. This has a direct effect on photodynamic therapeutic efficacy of nanosensitizers. Biocompatibility of these novel gold nanosensitizers *in vitro* was demonstrated and the potential of such novel nanosensitizers as multifunctional optical agents for cancer diagnosis and therapy was highlighted.

Keywords: SERS; Multimodality; Bioimaging; Oral cancer; Cell uptake

Introduction

Oral cancer is the sixth most common cancer worldwide [1]. In excess of 260,000 new cases are diagnosed annually, and with one of the lowest five year survival rates of all cancers (50%), the number of deaths from oral cancer recorded in 2008 was 127,654 [2]. Clinical examination and white light endoscopic imaging followed by histopathological analysis of needle biopsies remains the gold standard for the diagnostic surveillance of oral cancer, but has a limited diagnostic accuracy of <55%. Since biopsies are performed only when lesions appear abnormal, premalignant lesions can easily go undetected. Indeed, a study of new cases of oral and pharyngeal cancers in Ireland identified 60% of cases presenting with advanced disease (Stage III or Stage IV) due to late diagnosis [3]. Treatment options for patients with oral cancer include non-targeted surgery, chemotherapy and radiotherapy. Major disadvantages posed by the lack of discrimination between diseased and healthy tissue with such therapies include cytotoxicity, systemic toxicity, drug resistance, and often a necessity for reconstructive surgery. Because of this, the morbidity rate associated with conventional oral cancer treatment modalities is high. Hence, development of novel, minimally invasive, targeted diagnostic and treatment modalities for oral cancer are clearly warranted. Such advancements could provide a means of improving prognosis, patient survival outcomes and mortality rates, and in reducing health care costs [4].

In light of this, an area of considerable current interest in cancer research is the design of novel nanoagents that synergistically incorporate multiple functionalities (targeting, imaging, therapy) all within a single probe. Successful development of such multimodal

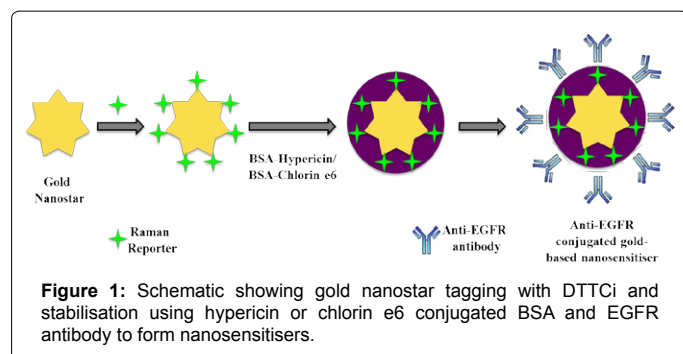
systems could permit the deployment of cancer therapy and diagnostics (theranostics) from the same platform. Gold nanoparticles (AuNPs) have been extensively investigated as a platform for multi-modal theranostics. The many applications of AuNPs depend on modifiable physical characteristics such as size, shape and surface chemistry. Favourable properties of AuNPs include ease of preparation, stability, efficient bioconjugation, tunable optical properties and biocompatibility [5]. AuNPs can be synthesized and seeded to form various shapes of various sizes including spheres, rods, triangles, cubes, platelets and stars. Changes in shape from spheres to rods and more anisotropic structures such as stars results in tuning of the surface plasmon resonance (SPR) from the visible to the near infrared (NIR) region (>600 nm) [6]. Minimal tissue autofluorescence and lower fluorescence extinction permit deeper tissue penetration and minimal background interference in this region [7]. The large scattering cross section of AuNPs can be exploited for detection by darkfield illumination [8]. AuNS exhibit intense localised surface plasmon resonance (LSPR) at their branch tips. LSPR induces a strong electromagnetic field in the region and

*Corresponding author: Malini Olivo, School of Physics, National University of Ireland, Galway University Road, Galway, Ireland, Tel: 65-6478-8732; E-mail: malini.olivo@nuigalway.ie, malini_olivo@sbic.a-star.edu.sg

Received October 21, 2014; Accepted November 26, 2014; Published December 05, 2014

Citation: Connolly JM, Raghavan V, Owens P, Wheatley A, Keogh I, et al. (2014) Nanogold-based photosensitizers probes for dual-model bioimaging and therapy of cancer. J Nanomed Nanotechnol 5: 249. doi: 10.4172/2157-7439.1000249

Copyright: © 2014 Connolly JM, et al. This is an open-access article distributed under the terms of the Creative Commons Attribution License, which permits unrestricted use, distribution, and reproduction in any medium, provided the original author and source are credited.



results in the electromagnetic enhancement of Raman signals. This resonant effect, known as surface enhanced Raman scattering (SERS), enhances Raman scattering efficiency up to 10^6 fold [9]. In addition to SERS, AuNSs can convert absorbed radiation to heat at the branch tips at SPR frequency, which can be exploited in an alternative form of cancer treatment, photothermal therapy (PTT) [10]. Complementary to these intrinsic properties, AuNPs can be further functionalized by bioconjugation to various ligands including Raman reporters, permitting surface enhanced Raman scattering (SERS) detection [11]; photosensitisers, permitting fluorescent-based photodynamic diagnosis (PDD) and photodynamic therapy (PDT) [12]; and tumour-specific biomarkers (e.g. epidermal growth factor receptor, EGFR), for tumour cell specificity and targeting [13]. In this way, AuNPs have been utilized in numerous biomedical applications as image contrast agents, diagnostic agents, nanosensors, therapeutic agents and drug delivery systems. AuNPs can be thus be tuned both optically and functionally for the application of interest, ultimately permitting the use of AuNPs for multi-modality imaging, diagnostic and therapeutic purposes.

Of critical importance for biomedical functionalisation of any nanoparticle (NP) is the highly efficient, specific delivery to the biological target in a biocompatible manner. A number of studies have been conducted to investigate AuNP uptake mechanisms, intracellular distribution, cytotoxicity and photo-mediated therapeutic efficacy. A recent study by Raghavan et al. demonstrated the biocompatibility and photodynamic and phototherapeutic efficacy of star-shaped nanosensitisers *in vitro* [10]. Visualisation of AuNP uptake using methods such as darkfield optical microscopy [8], Raman spectroscopy [11], fluorescence microscopy [12] and transmission electron microscopy (TEM) [14], and have demonstrated that AuNPs of various shapes (spheres, rods, stars) and sizes (1-100 nm) can be taken up into a variety of cell types. The kinetics of uptake and intracellular localisation are, however, dependent on AuNP shape, size, surface properties and cell type [14]. As such, an important consideration in the development of novel nanoprobe for cancer theranostic avenues is the characterisation of cellular uptake kinetics, intracellular localisation and associated therapeutic efficacy in the model system of interest.

Reported here is the synthesis and characterisation of novel multi-modal bioconjugated nanosensitisers (NS) as theranostic agents for oral cancer. Two such NS were developed by layering the photosensitisers hypericin (NS1) or chlorin e6 (NS2) onto multi-branched gold nanoparticles with a Raman reporter (DTTCi). Since overexpression of epidermal growth factor receptor (EGFR) is a hallmark of oral squamous cell carcinoma (OSCC), this could be taken as a putative predictive target for oral cancer [15]. Thus, the nanosensitiser complex was also bioconjugated to tumour-specific EGFR antibodies forming NS1-EGFR and NS2-EGFR. These novel NS were investigated for

efficacy as fluorescent and SERS-based optical diagnostic probes and as photodynamic and photothermal cancer therapeutic agents and demonstrated as potential multimodality agents for theranostics of oral cancer.

Materials and Methods

Materials

Unless specified otherwise, all materials were purchased from Sigma-Aldrich.

Nanosensitiser preparation

Nanosensitisers (NS) were synthesised as described previously [10] and complete protocols are provided in the supplementary information. Briefly, gold nanostars (AuNS) 30-50 nm was synthesized in the aqueous phase by reducing tetrachloroauric acid (HAuCl_4) with HEPES buffer. The Raman reporter, DTTi, was coated onto the AuNS. Photosensitisers (either hypericin or chlorin e6) conjugated with denatured BSA were then layered onto the DTTi-tagged AuNS. This nanosensitiser (NS) was then bioconjugated to an anti-epidermal growth factor receptor (EGFR) antibody (Figure 1).

NS characterisation

NS, once formed, were characterised using ultraviolet-visible (UV-vis) and fluorescence spectrometry, Raman spectroscopy and transmission electron microscopy (TEM). The UV-vis absorption measurements were performed with Shimadzu UV-2600. Fluorescence spectrometry was performed on the Shimadzu RF-5301. Surface enhanced Raman scattering (SERS) measurements were carried out with a Witec Alpha 500 Raman upright microscope using a 785 nm laser and 40x objective. NS morphology and size were examined using the Hitachi H7000 transmission electron microscope with accelerating voltage of 75 kV.

Cell culture

Two cell lines, SCC9 (a human tongue squamous cell carcinoma) and MCF7 (a human breast adenocarcinoma), were purchased from American Type Culture Collection (ATCC). Cells were cultured under standard conditions (5% CO_2 , 95% O_2 , 37°C) in Dulbecco's modified Eagle's medium (DMEM)/nutrient mixture F-12 Hams, phenol free supplemented with foetal bovine serum, L-glutamine, penicillin and streptomycin. Cells were seeded at a concentration of 5×10^5 cells/ml and were used for studies when they reached a confluency of approximately 70%. Depending on the study, cells were treated with different concentrations of NS (0-20 μM) for 3 or 24 hours and examined for cellular uptake, intracellular localisation, cytotoxicity, photodynamic and phototherapeutic therapy efficacy.

Cytotoxicity study

Cell viability was assessed following 24 hours treatment with various concentrations (0-20 μM) of NS1 or NS2 using the 3-(4,5-dimethylthiazol-2-yl)-2,5-diphenyl tetrazolium bromide (MTT) assay according to the manufacturer's instructions. Complete protocols are provided in the supplementary information.

Photodynamic Dynamic Therapy (PDT) study

Cells seeded at 5×10^3 cells per well in a 96-well plate were treated for 3 hours with 0-10 μM of NS1 or NS2. Medium was then replaced with fresh medium and cells were irradiated at a fluence of 1 J/cm². Following incubation in the dark for 18 hours, viability of the irradiated cells was assessed using the MTT assay.

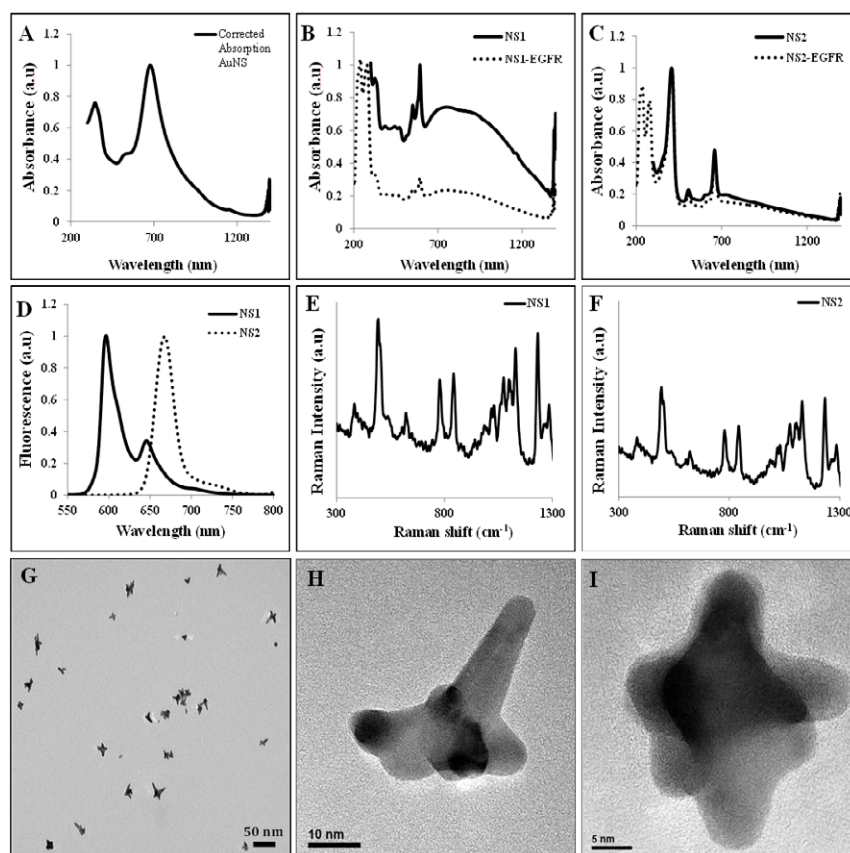


Figure 2: Characterisation of gold nanostars (AuNS) and nanosensitisers (NS): Figure 2 shows (A) the UV-Vis absorption spectra of multi-branched gold nanostars (AuNS); (B) the UV-Vis absorption spectra nanosensitisers NS1 and NS1-EGFR; (C) the UV-Vis absorption spectra NS2 and NS2-EGFR; (D) the fluorescence emission spectra for NS1 and NS2. The relevant emission peak for hypericin (590 nm) is seen in the spectra for NS1 and that for chlorin e6 (668 nm) in NS2; (E) Raman spectra for NS1 and (F) NS2 excited at 785nm laser excitation exhibiting characteristic spectral peaks of DTTc; TEM (G) and HR-TEM (H, I) images of synthesized 30-50 nm AuNS.

Photo Thermal Therapy (PTT) study

Cells seeded at 5×10^3 cells per well in a 96-well plate were treated with gold stars (AuNS) in order to examine photothermal therapeutic efficacy. The concentration of AuNS in contact with the cells was the same as in the complete NS levels used for PDT study (0-20 μ M). Following 3 hour treatment with AuNS, medium was replaced with fresh medium and cells were irradiated at a fluence of 1 J/cm². Following incubation in the dark for 18 hours, viability of the irradiated cells was assessed using the MTT assay.

NS uptake and intracellular localisation studies

NS uptake and intracellular localisation were assessed using darkfield contrast imaging, transmission electron microscopy, Raman spectroscopy and confocal fluorescence microscopy. Complete protocols are provided in the supplementary information.

Immunofluorescence staining and confocal imaging

Cells were treated with NS, fixed and processed for immunocytochemical staining as described in full in the supplementary information.

Image analysis

Cellular uptake of NS was quantified as the percentage area of

the cell that was occupied by NS. This was assessed using Image J by examination of the intensity of the fluorescence emission detected from cells treated with NS1, which contained the photosensitiser hypericin ($\lambda_{exc}=488$ nm; $\lambda_{em}=505$ nm) and NS2, which contained the photosensitiser Ce6 ($\lambda_{exc}=640$ nm; $\lambda_{em}=662$ nm). Colocalisation was assessed and quantified using the Image J plugin JACoP by examination of the intensity and ratio of fluorescence signals achieved from the NS and organelles fluorescent channels. This was calculated using Pearsons Colocalisation Coefficient (PCC), which depends on the amount of colocalized signals in both channels. PCC values range from -1 to 1, with 1 representing complete positive correlation, -1 representing negative correlation, and zero representing no correlation [16].

Results

Characterisation of gold stars and NS

The UV-Vis absorption spectra of multi-branched gold nanostars (AuNS) and nanosensitisers (NS1, NS2, NS1-EGFR and NS2-EGFR) are shown in Figures 2A-2C. The SPR peak for AuNS was visible at a wavelength of approximately 680 nm (Figure 2A). These AuNS were used to synthesise nanosensitisers (NS1 and NS2) and anti-EGFR bio-conjugated nanosensitisers (NS1-EGFR, NS2-EGFR). As shown in Figures 2B and 2C, the AuNS SPR peak (680 nm) was visible in these constructs, suggesting stable synthesis. In addition, both NS1-

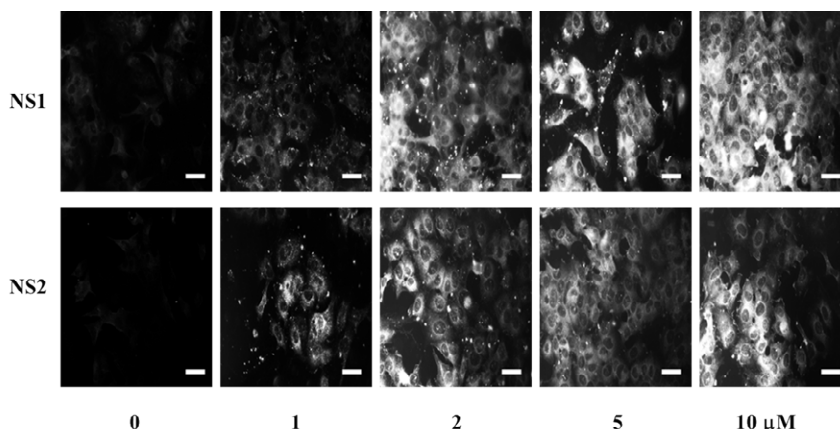


Figure 3: Darkfield image of SCC9 cells tagged with NS1 or NS2 (0-10 μM). Scale bar = 10 μm .

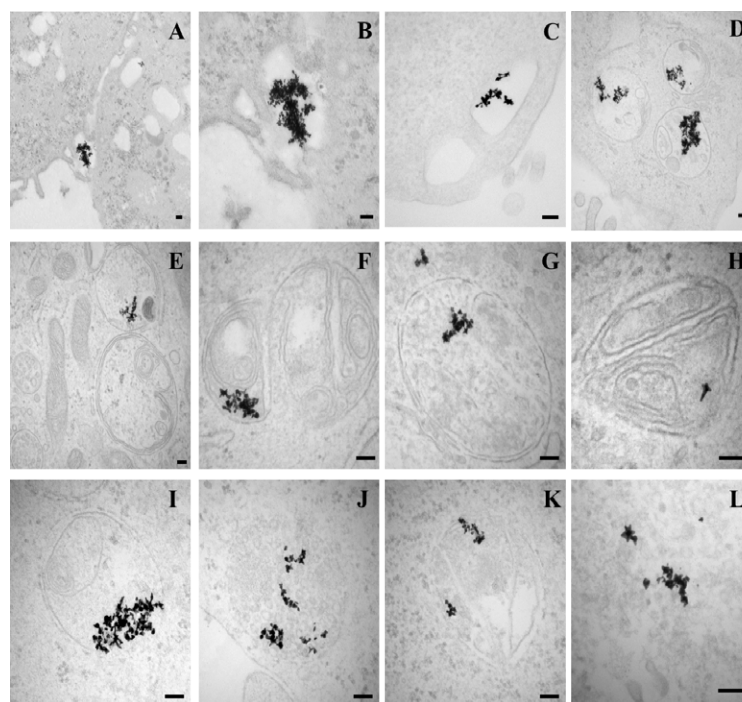


Figure 4: Transmission electron microscopy (TEM) micrographs showing positive NS1 (A-H) and NS2 (I-L) uptake into SCC9 cells and incorporation into intracellular vesicles. Scale bar = 100 nm.

EGFR and NS2-EGFR absorption spectra showed a peak at 280 nm. This corresponds to the relevant and characteristic protein absorption peak of EGFR antibody [15,17]. Fluorescence emission spectra for NS1 and NS2 are shown in Figure 2D. The relevant emission peak for hypericin (590 nm) was detected in NS1 and that for Ce6 (668 nm) was detected in NS2. Surface enhanced Raman spectral (SERS) properties of nanosensitizers were examined at 785 nm laser excitation. The characteristic Raman spectral peaks of DTTCi were detectable in both NS1 and NS2 with similar SERS intensities and are shown in Figures 2E and 2F. Figures 2G-2I shows TEM and HR-TEM images of synthesized AuNS. From these images, AuNS were generally present in a monodispersed state with minimal aggregation. AuNS range in size from 30-50 nm and have an average branch number of 4.

Imaging and quantification of *in vitro* uptake of NS

In vitro uptake and intracellular distribution of NS was observed using darkfield contrast imaging, transmission electron microscopy (TEM), confocal fluorescence microscopy and Raman spectroscopy. For all imaging studies, cells were incubated with NS for 3 or 24 hours at various concentrations (1-10 μM), fixed and processed. *In vitro* localisation of NS using darkfield contrast imaging showed a dose-dependent uptake into SCC9 cells following a 3 hour incubation period (Figure 3), with more NS present in cells treated with 10 μM compared to 0-5 μM . Although not quantified from these images, NS1 appeared to be taken into the cells at an increased rate compared to NS2 (Figure 3).

NS uptake and intracellular localisation was further examined

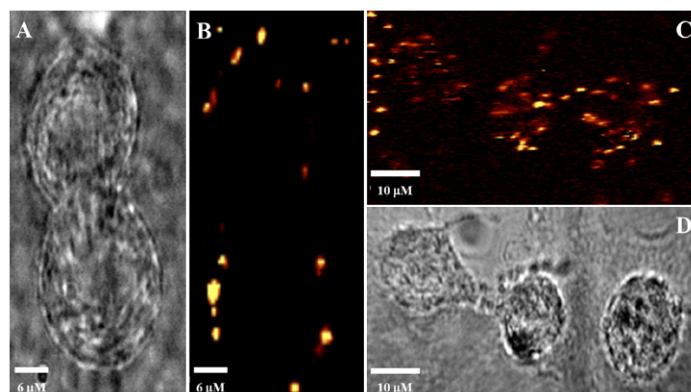


Figure 5: *In vitro* SERS mapping results following 3 hour treatment with NS1 (A, B) and NS2 (C, D) on SCC9 cells. Figure 5 shows brightfield images (A, D) and corresponding cell SERS images (B, C) created using the sum filter from the 1214- 1260 cm^{-1} peaks of the attached Raman reporter, DTTCi, at 785 nm laser excitation.

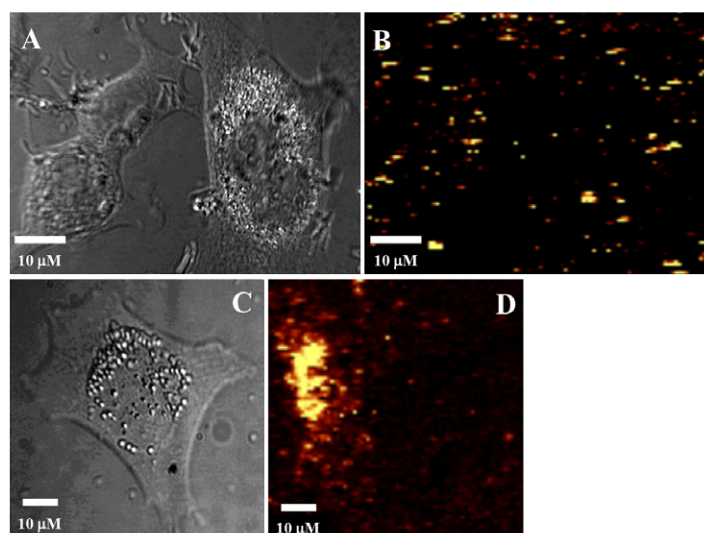


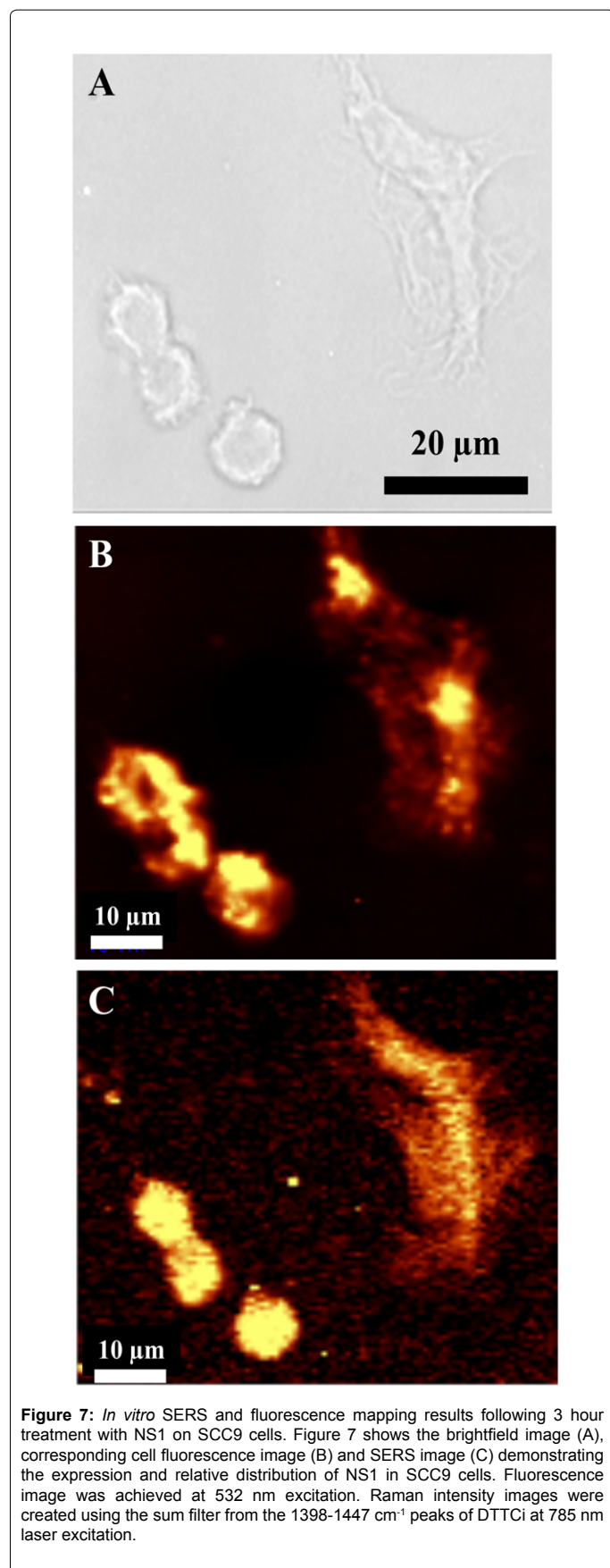
Figure 6: *In vitro* SERS mapping results following 3 hour treatment with NS1 (A, B) and NS2 (C, D) on MCF7 cells. Figure 6 shows brightfield images (A, C) and corresponding cell SERS images (B, D) created using the sum filter from the 1214- 1260 cm^{-1} peaks of the attached Raman reporter, DTTCi, at 785 nm laser excitation.

using transmission electron microscopy. Figure 4 confirms the data from darkfield imaging that both NS were successfully taken up into cells. The internalisation process of NS1 and NS2 appeared to be an endocytotic mechanism, as suggested by the extension of pseudopodia and internalisation of nanoparticles into large intracellular vesicles (Figures 4A-4C). Both NS1 and NS2 redistributed intracellularly to various membrane bound cytoplasmic organelles and were clearly visible following 24 hour treatment in endosome-lysosome like structures, as well as to double-membrane phagosomes or autophagosomes (Figures 4D-4K). NS2 also appeared to locate to the cytoplasm, and was often seen not to be associated with any organelles or membrane bound vesicles (Figure 4L). No NS could be visualised within the nucleus of any cells.

Additional *in vitro* optical imaging in the form of SERS mapping of NS was possible owing to the presence of the Raman reporter, DTTCi on NS1 and NS2. Brightfield and cell SERS images of SCC9 and MCF7 cells treated with NS1 and NS2, along with the corresponding SERS

spectra for NS1 and NS2 are shown in Figures 5 and 6. Here, NS uptake and intracellular localisation were shown in the SERS mapping images at the respective characteristic Raman peak range for DTTCi of 1214-1260 cm^{-1} . This study provides further verification of NS uptake into cells. From these images, NS again appears to be taken up in a more selective and higher rate in SCC9 cells compared to MCF7 cells (Figures 5 and 6). Raman-based detection of NS1 and NS2 in cells confirm the usefulness of these novel NS as SERS nanopobes.

While NS uptake was not quantified from the Raman images, the presence of the fluorescent photosensitizers hypericin on NS1 and NS1-EGFR and Ce6 on NS2 and NS2-EGFR permitted the utilisation of confocal fluorescence microscopy for examination of NS uptake into cells. In a study to examine the functionality of NS in terms of both fluorescence and Raman capabilities, a single group of cells treated with NS were imaged. Results from this study demonstrate a clear overlap between Raman and fluorescent signals (Figure 7). Therefore, quantification of confocal fluorescence intensity could be taken as



an estimation of Raman intensity and the function of these novel NS as dual-modal nanoprobe capable of emitting strong Raman and fluorescent signals that were detectable in cells was confirmed.

In order to quantify NS uptake, SCC9 and MCF7 cells were treated with 1 μM of NS1, NS2, NS1-EGFR or NS2-EGFR for 3 hours. Confocal fluorescent images of cells treated with hypericin-containing NS1 and NS1-EGFR and with Ce6-containing NS2 or NS2-EGFR are shown in Figures 8 and 9. With an absorption emission of 590 nm, hypericin fluorescence is visible in the red region, while Ce6, with an absorption emission of 668 nm, fluoresces in the far-red region. As shown in darkfield, TEM and Raman images, confocal images also demonstrated that NS1 and NS2 were taken up into SCC9 and MCF7 cells. The uptake of NS1 again appeared to exceed that of NS2 (Figure 8A and 8I). Using the confocal fluorescence images for examination of the mean fluorescence intensity (MFI) signals from the conjugated photosensitizers (hypericin and Ce6), it was possible to quantify the uptake of the NS in cells. This quantification was expressed as a percentage of cell area occupied by NS (% cell area). In addition, due to the presence of anti-EGFR antibodies on NS1-EGFR and NS2-EGFR, it was also possible to quantify and compare the effect of antibody conjugation on NS uptake specificity between the two cell lines.

Results from this study are shown in Figures S1 and S2 in supplementary information. Quantification of the mean fluorescence intensity of NS fluorescence signal showed approximately 3% of SCC9 cell area when treated with NS (1 μM , 3 hours) was occupied by NS1, while NS2 occupied approximately 10 times less of the cells area (0.3%) ($P < 0.01$). A similar result was observed in MCF7 cells with approximately 9 times more NS1 occupying the percentage cell area (1.9%) compared to NS2 (0.2%) ($P < 0.01$). Bioconjugation of EGFR to NS also affected uptake in a cell- and photosensitizer-dependent manner. In SCC9 cells, bioconjugation of NS to EGFR had no significant effect on the uptake of NS compared to NS without antibody. NS1-EGFR occupied significantly more (3.2%) of the percentage SCC9 cell area than NS2-EGFR (0.4%) ($P < 0.01$). In MCF7 cells, similar to the differential uptake of NS1 and NS2, NS1-EGFR was shown to occupy approximately 4 times more of the percentage cell area (0.4%) compared to NS2-EGFR (0.1%) ($P < 0.05$). Significantly less NS1-EGFR was taken into the cell compared to NS1 (without antibody) (0.4 v 1.9%) ($P < 0.05$). The uptake of NS2 and NS2-EGFR by MCF7 cells was shown to be similarly low (0.1%). In summary, NS appeared to exert some cell specificity, with a higher rate of entry into SCC9 cells compared to MCF7 cells evident. A photosensitizer-mediated effect on uptake was demonstrated by the observation that NS1 was taken into both cell types at a significantly higher rate than NS2. Furthermore, bioconjugation of EGFR antibody had no positive effect on NS2 uptake in either cell line, but did significantly impede NS1 uptake (NS1-EGFR) into MCF7 cells.

***In vitro* colocalisation of NS with intracellular organelles**

Results from previous studies confirmed using multiple modalities (darkfield, TEM, confocal fluorescence and Raman spectroscopy) that these novel NS are capable of entering cells. TEM images (Figure 4) showed that, 24 hours after treatment, NS had distributed intracellularly to the cytoplasm and to membrane bound vesicles of the endosome-lysosome pathway. In order to investigate where in the cell NS colocalised to within 3 hours of treatment, intracellular colocalisation of NS with various organelles (mitochondria, lysosomes, endoplasmic reticulum, Golgi apparatus) was examined in SCC9 and MCF7 cells quantitatively using Pearson's correlation coefficient (PCC) calculation on confocal fluorescent images. Cells treated with 1 μM of NS1, NS2, NS1-EGFR or

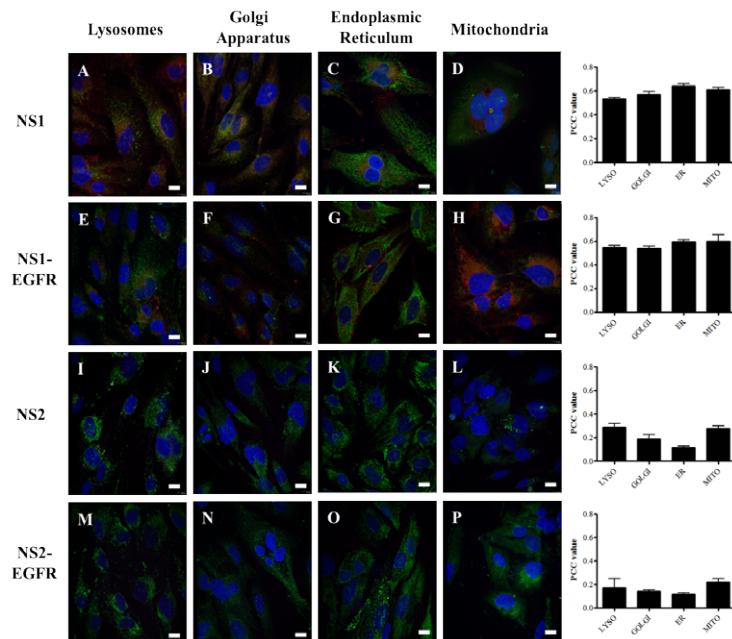


Figure 8: Nanosensitiser colocalisation with various organelles in SCC9 cells: images and analysis. SCC9 cells were immunohistochemically labelled green for lysosomes, Golgi apparatus, endoplasmic reticulum or mitochondria. NS1 and NS1-EGFR contain the photosensitiser hypericin and localisation is depicted in the images in red (A-H). NS2 and NS2-EGFR contain the photosensitiser chlorin e6 and localisation is depicted in the micrographs in far red (I-P). Nuclei were counter-stained with Hoechst (blue). Positive nanosensitiser colocalisation with organelles is indicated by yellow-orange areas. Images were taken at 40x with an oil immersion lens. Scale bar=10 μ m.

Graphs on the right hand side depict quantification of colocalisation of the 4 nanosensitisers with endoplasmic reticulum (ER), lysosomes, Golgi apparatus and mitochondria. Colocalisation was quantified by calculating Pearson's Correlation Coefficient (PCC). The PCC values for this are shown here. n=60-200.

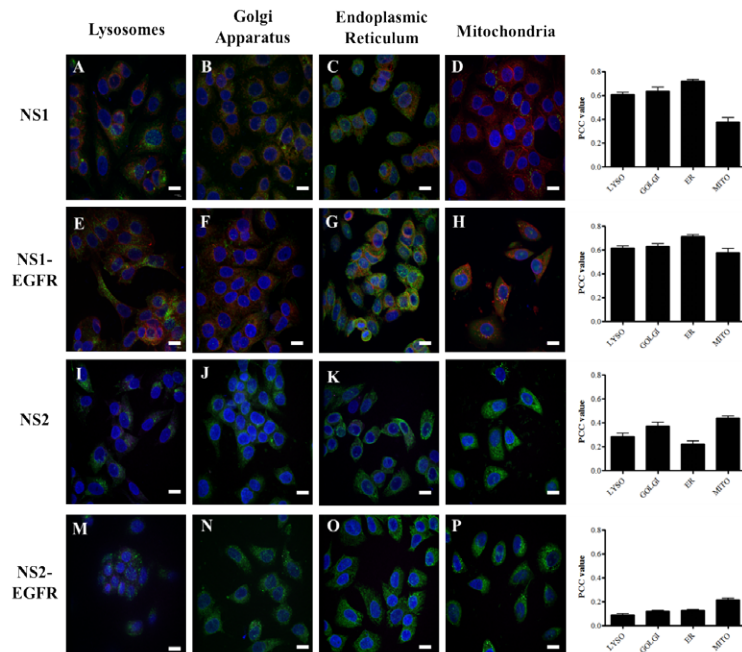


Figure 9: Nanosensitiser colocalisation with various organelles in MCF7 cells: images and analysis. MCF7 cells were immunohistochemically labelled green for lysosomes, Golgi apparatus, endoplasmic reticulum or mitochondria. NS1 and NS1-EGFR contain the photosensitiser hypericin and localisation is depicted in the images in red (A-H). NS2 and NS2-EGFR contain the photosensitiser chlorin e6 and localisation is depicted in the micrographs in far red (I-P). Nuclei were counter-stained with Hoechst (blue). Positive nanosensitiser colocalisation with organelles is indicated by yellow-orange areas. Images were taken at 40x with an oil immersion lens. Scale bar=10 μ m.

Graphs on the right hand side depict quantification of colocalisation of the 4 nanosensitisers with endoplasmic reticulum (ER), lysosomes, Golgi apparatus and mitochondria. Colocalisation was quantified by calculating Pearson's Correlation Coefficient (PCC). The PCC values for this are shown here. n=60-200.

NS2-EGFR for 3 hours were fixed and immunocytochemically labelled (green) with antibodies and dyes specific for various organelles (Table S1, in supplementary information). Micrographs of SCC9 and MCF7 cells double-stained with fluorescent photosensitisers in NS1 and NS2 (hypericin and Ce6, respectively) and antibodies or dyes specific for organelles are shown in Figures 8 and 9, respectively. Quantification of the colocalisation of NS with various organelles was calculated using PCC. Data from this analysis was graphed and is shown in Figures 8 and 9.

In both cell lines, hypericin and Ce6 fluorescence were mainly detected in the perinuclear region, with little fluorescence detected in the nucleus. This was in agreement with TEM studies, where NS was not found in the nucleus of any cells. As in the uptake study, intracellular distribution and colocalisation of NS with organelles appeared to be cell-type and photosensitiser-type dependent. In SCC9 cells, there was no significant difference in the intracellular localisation of NS1 and NS1-EGFR, with both NS colocalising to mitochondria, Golgi apparatus, ER and lysosomes in a similar fashion) with an associated Pearson's coefficient value of approximately 0.6 in all cases (Figures 8A-8H). In correlation with results in the uptake study (Figures S1 and S2, supplementary information), NS2 and NS2-EGFR colocalised to organelles to a lesser extent than NS1 or NS1-EGFR as shown by PCC values of <0.3 (compared to 0.6). No difference was observed in the colocalisation of NS2 and NS2-EGFR to organelles in SCC9 cells, with an associated Pearson's coefficient value of approximately 0.3 in all cases.

In MCF7 cells (Figures S1 and S2, supplementary information), significantly more NS1 localised to organelles compared to NS2, regardless of bioconjugation to EGFR (Figure 9). Both NS1 and NS1-EGFR were shown to colocalise preferentially to endoplasmic reticulum ($P < 0.05$). Similar levels of colocalisation of NS1 and NS1-EGFR were seen in the Golgi apparatus and lysosomes; however significantly more NS1-EGFR was found in mitochondria compared to NS1 (PCC values 0.7 v 0.4). Significantly more NS2 was shown to be localised to all organelles compared to NS2-EGFR ($p < 0.01$). Both NS2 and NS2-EGFR appeared to preferentially locate to mitochondria in comparison to all other organelles examined.

Cell toxicity assay

The cytotoxic effect of NS (0-10 μM) and AuNS (gold nanostars) on SCC9 and MCF7 cells was assessed following 24 hour incubation using an MTT assay and results are shown in Figure S3A and S3B in the supplementary information. Compared to non-treated controls, no significant cytotoxic effects on the cells following 24 hours incubation with NS1, NS2 or AuNS at any of the levels tested were detected.

Photodynamic and photothermal therapy

To assess NS efficacy as a phototherapeutic agent, cells were treated with either NS1 or NS2 (0-10 μM) for 3 hours and irradiated at a fluence of 1 J/cm^2 . Percentage cell viability compared to non-treated controls was assessed using the MTT assay. A significant PDT effect of 2-5 μM NS1 in both SCC9 and MCF7 cells was observed ($p < 0.05$) (Figure S3C and S3D in the supplementary information). NS2 had a significant PDT effect on MCF7 cell viability at 5 and 10 μM concentration (Figure S3D in the supplementary information). AuNS had a significant PTT effect on SCC9 cells at all concentrations (1-10 μM); however no significant PTT effect was demonstrated in MCF7 cells at the AuNS concentrations and fluence rates examined in this study.

Discussion

Currently, most oral cancer diagnoses occur at the advanced disease stages owing to the reliance on detection of morphological and structural changes at the tissue level detected by conventional histopathological methods. Standard protocols for oral cancer treatment include invasive surgery, followed by chemotherapy or radiation therapy, all of which are associated with significant side effects and high morbidity [1-3]. Development of novel, minimally invasive, targeted diagnostic and treatment modalities are clearly warranted. Such systems could potentially synergistically incorporate multiple functionalities (targeting, imaging, therapy) within a single nanoprobe; in this way, cancer therapy and diagnostics (theranostics) could be deployed from the same platform [4]. This area is one of considerable current research interest and many important advances relating to multimodal approaches for theranostics have been made in recent years. As such, many options (the choice of base nanomaterial, e.g. up-conversion nanomaterials, carbon nanodots, nanometals; choice of fluorescent molecule; choice of photosensitiser; whether encapsulation of the fluorescent molecule is necessary; addition of an intracellular targeting moiety) exist when attempting to fabricate novel nanoprobe. These choices ultimately depend on the intended use and functionality of the nanoprobe. Like the other nanomaterials aforementioned, AuNPs have been extensively investigated as such multi-modality theranostic platforms [10,17]. Here we describe further the functionalisation of AuNPs to form nanosensitisers (NS) with multimodal diagnostic imaging capabilities (fluorescence, surface enhanced Raman spectroscopy (SERS)) and therapeutic efficacy (photodynamic therapy (PDT) and photothermal therapy (PTT)), and the characterisation of the potential use of these NS for oral cancer diagnosis and treatment. In particular, this study investigated the *in vitro* cellular uptake and intracellular localisation of NS in both an oral cancer (SCC9) and breast cancer cell line (MCF7).

In the current study, gold nanostars (AuNS) of approximately 30-50 nm in diameter with an average branch number of 4 (Figures 2G-2I) and a surface plasmon resonance (SPR) peak at the NIR wavelength of 680 nm (Figure 2A) were stably synthesised. The light scattering property of gold nanoparticles was exploited in this study and used to image NS cellular uptake by darkfield illumination (Figure 3). Using this technique, NS uptake into cells was confirmed and a dose-dependent effect on uptake was observed. The SERS capability of AuNS was exploited further in this study to facilitate molecular optical imaging and detection via conjugation of a Raman reporter (e.g. DTTCi). There are many advantages of using SERS as an optical technique over traditional technologies like fluorescence. These include high specificity, enhanced sensitivity and stability [5]. SERS has been successfully used in *in vitro* cell imaging and in *in vivo* targeted imaging and multiplex detection of cancer in xenograft tumour models [17]. SERS capabilities of NS1 and NS2 are highlighted in figures 2E and F where the characteristic peaks of bioconjugated Raman reporter DTTCi is shown. Successful SERS imaging of SCC9 and MCF7 cells treated with NS are shown in Figures 5-7, thus confirming the use of these novel NS as SERS nanotags.

In addition to SERS diagnostics, further functionalisation of the NS in terms of optical diagnostic imaging capabilities was possible in the current study owing to the presence of fluorescent photosensitisers (hypericin, Ce6) on NS1 and NS2. Photosensitisers are light-absorbing compounds activated to emit fluorescent light once activated by exposure to light of a specific wavelength. Such photodynamic diagnosis (PDD) has been widely utilised for tissue visualisation, cancer diagnosis and tumour detection [13,18]. Essential criteria for fluorescent agents

suitable for cancer imaging include adequate penetration depth for imaging regions deep within the body, emission of a strong, detectable fluorescence signal and malignant tissue specificity. Fluorophores, including Ce6 absorbing in the NIR region have shown great potential in this regard owing to their low autofluorescence and deep light penetration in tissues [18]. Fluorescence emission spectra for NS1 and NS2 (Figure 2) show the relevant emission peaks for hypericin (590 nm) and Ce6 (668 nm), respectively. Fluorescent imaging of cells treated with NS was performed using confocal fluorescence and confirmed the fluorescent detection of NS within cells. Successful SERS imaging and comparison to fluorescence imaging in a group of cells is shown in Figure 7. This confirms the successful development of novel NS probes capable of dual fluorescent and SERS detection and imaging in cancer cells.

The fluorescent properties of NS1 and NS2 were exploited in this study to examine and quantify cell uptake and intracellular colocalisation with various organelles using immunocytochemistry and confocal fluorescence microscopy. Of interest here was the comparison of uptake between NS1 and NS2, and also the effect of bioconjugation of EGFR antibodies to the NS complex on NS uptake. Over-expression of EGFR is a hallmark of oral cancer and is linked to aggressive tumour behaviours [15]. The oral cancer model used in this study (SCC9 cell line) was thus EGFR positive, while the MCF7 breast cancer cell line was EGFR negative. Thus, quantification of uptake of NS with and without antibody in this *in vitro* study could give an indication as to the usefulness of antibody bioconjugation in terms of cell specific receptor-targeting for cancer detection and discrimination between malignant and benign tissue. Nanoparticles are internalized via a number of mechanisms including diffusion, phagocytosis, pinocytosis and receptor-mediated endocytosis (RME). Small, hydrophobic and positively charged NPs such as carbon nanotubes or quantum dots (QDs) have been reported to enter cells by diffusion. RME pathways include caveolae- and clathrin- dependent and independent mechanisms. The general consensus regarding the mechanism of AuNP uptake is that RME predominates for particles <100 nm [19]. Indeed, the TEM results from this study suggest active endocytotic uptake of nanoparticles into cells, as well as the colocalisation of NS to the endosomal-lysosomal pathway (Figure 4).

Results from this study showed that EGFR bioconjugation to NS had no effect on NS uptake into SCC9 cells or on the uptake of NS2 into MCF7 cells. However, EGFR bioconjugation did significantly impede entry of NS1 into MCF7 cells ($P < 0.01$). Thus, in this study, EGFR did not enhance NS uptake into EGFR-positive cells, but restricted entry into EGFR negative cells (Figures S1 and S2, supplementary information). This is likely due to restricted cell entry owing to the large size of the NS-EGFR complex. In the *in vivo* situation, such a size dependence on uptake could act to promote uptake in malignant compared to benign tissue owing to the enhanced permeability and retention (EPR) effect. Thus, some degree of selectivity and targeting of delivery of NS by a receptor-targeted approach was shown here. In addition to this, NS1 was shown to enter cells at a significantly higher rate (> 9 fold) than NS2 ($P < 0.01$). The primary distinction between NS1 and NS2 is the presence of different photosensitisers in the NS complex; hypericin in NS1 and Ce6 in NS2. This could be taken to suggest therefore, that the rate of NS uptake is dependent on the photosensitiser present. Indeed, uptake and intracellular localisation of photosensitisers has been extensively studied and found to be dependent on the chemical properties of the sensitiser. Such properties include hydrophobicity and charge [20]. As a negatively charged and lipophilic molecule, hypericin likely enters cells by diffusion and has been shown to predominantly localise to cellular

membrane systems [21]. Ce6 is a porphyrin-based second generation photosensitiser. With an absorbance in the far-red spectral region (668 nm), Ce6 is somewhat superior to hypericin in terms of depth of penetration [22]. While the general consensus is that Ce6 is taken up into cells by passive membrane diffusion and tends to concentrate at the surface of membranes with minimal electrostatic drive to actually traverse them, in a study examining Ce6 uptake while utilising endocytotic-inhibitory temperatures (2°C), uptake was reduced, thus suggesting that Ce6 uptake was via pinocytosis [23]. In a recent study, HeLa cells incubated with Ce6 for 2 hours showed very little cell entry owing to the large negative charge on Ce6, while binding of Ce6 to gold nanorods (AuNR) with a subsequent increase in zeta potential facilitated cell entry via endocytosis [24]. Thus, at the concentration (1 µM) and treatment duration (3 hours) used in this present study, it is possible that the negative charge on Ce6-containing NS2 exceeded that on hypericin-containing-NS2, thus acting as an inhibitor to uptake, and may explain the reduced uptake of NS2 compared to NS1.

An additional consideration when examining nanoparticle uptake is the subsequent intracellular trafficking. Once internalized, the intracellular redistribution of NPs is an important consideration in terms of nanoparticle function. In relation to this, the localisation of NPs in the cell is dependent on the mode of cellular uptake. NPs taken up by endocytotic mechanisms are packaged in endosomes and redistributed to organelles including mitochondria, Golgi apparatus, and endoplasmic reticulum (ER). Alternatively, NPs are trafficked to lysosomes and transported to the cell surface for exocytosis [25]. TEM images (Figure 4) showed that, 24 hours after treatment, NS had distributed intracellularly to the cytoplasm and to membrane bound vesicles of the endosome-lysosome pathway, and also to autophagosomes. Since these vesicles are involved in the degradation of cellular material, it is possible that 24 hours after treatment, the cell is beginning to package the AuNP complex for excretion and exocytosis [19]. In order to investigate and quantify intracellular distribution of NS prior to cell packaging for removal, and to examine the target of NS once taken up into the cell, the colocalisation of NS with lysosomes, mitochondria, Golgi apparatus and ER were examined within 3 hours of treatment using immunocytochemistry and confocal microscopy. Quantification of colocalisation was performed using Pearson's Colocalisation Coefficient (PCC). PCC values vary from +1 to -1. In the case of a perfect positive linear relationship (correlation), PCC value would be +1. In the case of a perfect negative linear relationship (autocorrelation), PCC value would be -1. A PCC value of 0 represents the case of no relationship (uncorrelated) [26]. In agreement with previous studies [27,28], NS appeared to distribute primarily to the perinuclear region and were found to localise to Golgi apparatus, mitochondria, lysosomes and ER. NS1 was found to colocalise equally among all organelles in both cell lines, while NS2 preferentially located to mitochondria and lysosomes. As reported by other groups, it appears here that the intracellular localisation of NS was dependent on both the nature of the photosensitiser and on cell-type [20]. In a study by Woodburn et al. examining the effect of photosensitiser hydrophobicity and charge on intracellular localisation, it was found that cationic photosensitisers were found in mitochondria while anionic photosensitisers were found in lysosomes [29]. In a study by Ritz et al. hypericin was found to localise to the ER and Golgi apparatus in glioblastoma cells [30]. In human nasopharyngeal carcinoma cells, the intracellular localisation of hypericin was shown to be the mitochondria and lysosomes [27]. Ce6, on the other hand was found to colocalise to the plasma membrane of human fibroblasts [28] and to ER, Golgi apparatus, mitochondria and lysosomes in MCF7 cells [31]. Of interest here is the disparity between

the TEM images which showed NS primarily located in endosomes and lysosomes, while the confocal fluorescence images showed NS in other organelles. There are two possible explanations for this; the TEM images were taken 24 hour after treatment, and at this stage NS may have entered the endosome-lysosomal pathway for cellular excretion. Alternatively, the fluorescent photosensitisers may become dissociated intracellularly from the AuNP core of the NS complex. While further studies will be necessary to examine more closely the behavior and kinetics of the components of the NS following internalization, the chemical nature of photosensitisers in such NS should be taken into account, and could represent a method of intracellular targeting.

The importance of intracellular localisation of nanoparticles is related to the photodynamic therapeutic function of the associated photosensitisers and the photothermal therapeutic function of the associated AuNS core. Photosensitisers, when irradiated with light corresponding to an absorbance optimum for the photosensitiser, cause an energy transfer process which results in the conversion of molecular oxygen to reactive oxygen species (ROS). Depending on the type of reaction (type I or II), either superoxide radicals or singlet oxygen molecules (1O_2) are formed, respectively. The excessive production of ROS causes oxidation of many biomolecules (proteins, lipids), oxidative stress and ultimately cell death via apoptotic, necrotic or autophagic mechanisms, provided there is sufficient light, oxygen and photosensitising agent available [32]. However, these species have an extremely short half-life and diffuse poorly in biological environments. Thus, the area affected by photo-induced damage is limited to the cell structures in close proximity to the photosensitiser. Hence, the subcellular localisation of the photosensitisers is a major factor governing the extent of PDT mediated cell damage and subsequent cell death [32,33]. Mitochondrial photodamage elicits a chain of pro-apoptotic events including loss of mitochondrial membrane potential, increased mitochondrial permeability, release of cytochrome c and activation of caspases, leading to apoptotic cell death [33]. As such, some groups have reported surface modification of nanoparticles with the mitochondriotropic ligand triphenylphosphonium (TPP), enabling mitochondrial targeting [34]. ER stress in the form of Ca^{2+} storage or protein handling disturbances as can be induced by photodamage represents an additional pathway to cell apoptosis. In terms of lysosomes, membrane damage can lead to necrosis. In addition, studies have shown that exposure of cells to light can cause release of lysosomal contents, thus permitting redistribution of photosensitiser to other intracellular targets [33].

NS1 was shown here as a viable phototherapeutic agent capable of exerting 50% cell death in SCC9 cells and 30% cell death in MCF7 cells following treatment at a level of 2-10 μ M with a subsequent 1 J/cm² laser fluence. On the other hand, NS2 had no significant PDT effect on SCC9 cells, but did exert 20-30% cell death in MCF7 cells at 5-10 μ M levels and 1 J/cm² laser fluence. These results correlate well with the uptake study, which demonstrated a significantly (30%) higher rate of uptake of NS1 into SCC9 compared to MCF7 cells, thereby conferring a larger PDT potential in SCC9 cells. Furthermore, in examination of the relatively low uptake of NS2 (<0.3%) compared to NS1 (<2%), one might expect the observed reduction in PDT efficacy owing to reduced available photosensitiser concentration.

In terms of photothermal therapy (PTT), AuNS had a significant PTT effect on SCC9 cells only. This may again be explained by the increased uptake of NS into SCC9 cells compared to MCF7 cells and also to optimisation of the fluence rates and duration for SCC9 cells

in this study. This provides further evidence of NS ability to non-specifically target different cells types and stresses the importance of *in vitro* studies in multiple cell lines in order to functionally characterise the NP of interest.

Conclusion

The development of novel agents capable of minimally invasive and targeted theranostics of oral cancer is critical for improving patient outcome. Here we describe the successful fabrication of novel nanogold based theranostic photosensitiser probes (nanosensitisers) capable of multi-modal bioimaging and therapy in an oral cancer cell model. The endowment of NS with receptor-targeting capabilities by bioconjugation to EGFR antibodies altered the uptake of NS in a cell type-dependent fashion, by impeding entry to EGFR-negative cells. In examination of the uptake and intracellular distribution of NS in oral and breast cancer cells, both photosensitiser-type and cell-type dependent mechanisms were apparent. Furthermore, in comparing the confocal fluorescent and electron microscopy data relating to intracellular localisation, a post-uptake dissociation of photosensitiser from the AuNS complex could be taken to explain the disparity in NS colocalisation with organelles. The NS were shown to be biocompatible and capable of ensuing cell death following PDT and PTT, and the efficacy of photo-mediated cell damage correlated well with both the degree of cell uptake and intracellular localisation. While highlighting the necessity of investigation at the cellular level the uptake and intracellular distribution of nanoparticles for a more complete biomedical and functional characterisation of novel nanosensitisers, this study also demonstrates the potential benefit of such novel nanogold-based multi-modality platforms for successful theranostics in cancer.

Funding

This work was supported by Science Foundation Ireland (SFI).

References

1. Warnakulasuriya S (2009) Global epidemiology of oral and oropharyngeal cancer. *Oral Oncol* 45: 309-316.
2. Khalili J (2008) Oral cancer: risk factors, prevention and diagnostic. *Exp Oncol* 30: 259-264.
3. O'Sullivan EM (2005) Oral and pharyngeal cancer in Ireland. *Ir Med J* 98: 102-105.
4. Olivo M, Bhuvaneshwari R, Keogh I (2011) Advances in bio-optical imaging for the diagnosis of early oral cancer. *Pharmaceutics* 3: 354-378.
5. Cai W, Gao T, Hong H, Sun J (2008) Applications of gold nanoparticles in cancer nanotechnology. *Science and Applications* 19: 17-32.
6. Huang X, El-Sayed IH, El-Sayed MA (2010) Applications of gold nanorods for cancer imaging and photothermal therapy. *Methods Mol Biol* 624: 343-357.
7. Yi X, Wang F, Qin W, Yang X, Yuan J (2014) Near-infrared fluorescent probes in cancer imaging and therapy: an emerging field. *Int J Nanomedicine* 9: 1347-1365.
8. Curry AC, Crow M, Wax A (2008) Molecular imaging of epidermal growth factor receptor in live cells with refractive index sensitivity using darkfield microspectroscopy and immunotargeted nanoparticles. *The Journal of Biomedical Optics* 13: 014022.
9. Willets KA, Van Duyne RP (2007) Localized surface plasmon resonance spectroscopy and sensing. *Annu Rev Phys Chem* 58: 267-297.
10. Raghavan V, Connolly JM, Fan HM, Dockery P, Wheatley A, et al. (2014) Gold nanosensitisers for multimodal optical diagnostic imaging and therapy of cancer. *Journal of Nanomedicine & Nanotechnology* 5: 238.
11. Shah NB, Dong J, Bischof JC (2011) Cellular uptake and nanoscale localization of gold nanoparticles in cancer using label-free confocal Raman microscopy. *Mol Pharm* 8: 176-184.

12. Mieszawska AJ, Mulder WJ, Fayad ZA, Cormode DP (2013) Multifunctional gold nanoparticles for diagnosis and therapy of disease. *Mol Pharm* 10: 831-847.
13. Olivo M, Lucky SS, Bhuvaneshwari R, Dendukuri N (2011) Nanosensitizers for multi-modality optical diagnostic imaging and therapy of cancer. *Proceedings of SPIE-OSA Biomedical Optics* 8087: 1-12.
14. Chithrani BD, Stewart J, Allen C, Jaffray DA (2009) Intracellular uptake, transport, and processing of nanostructures in cancer cells. *Nanomedicine* 5: 118-127.
15. Laimer K, Spizzo G, Gastl G, Obrist P, Brunhuber T, et al. (2007) High EGFR expression predicts poor prognosis in patients with squamous cell carcinoma of the oral cavity and oropharynx: a TMA-based immunohistochemical analysis. *Oral Oncol* 43: 193-198.
16. Dinish US, Balasundaram G, Chang YT, Olivo M (2014) Actively targeted in vivo multiplex detection of intrinsic cancer biomarkers using biocompatible SERS nanotags. *Sci Rep* 4: 4075.
17. Chin WW, Thong PS, Bhuvaneshwari R, Soo KC, Heng PW, et al. (2009) In-vivo optical detection of cancer using chlorin e6-polyvinylpyrrolidone induced fluorescence imaging and spectroscopy. *BMC Med Imaging* 9: 1.
18. Shukla R, Bansal V, Chaudhary M, Basu A, Bhonde RR, et al. (2005) Biocompatibility of gold nanoparticles and their endocytotic fate inside the cellular compartment: a microscopic overview. *Langmuir* 21: 10644-10654.
19. Berg K, Moan J (1997) Lysosomes and microtubules as targets for photochemotherapy of cancer. *Photochem Photobiol* 65: 403-409.
20. Uzdensky AB, Ma LW, Iani V, Hjortland GO, Steen HB, et al. (2001) Intracellular localisation of hypericin in human glioblastoma and carcinoma cell lines. *Lasers Med Sci* 16: 276-283.
21. Moon YH, Kwon SM, Kim HJ, Jung KY, Park JH, et al. (2009) Efficient preparation of highly pure chlorin e6 and its photodynamic anti-cancer activity in a rat tumor model. *Oncol Rep* 22: 1085-1091.
22. Roberts W, Berns M (1989) *Cell Biology and Photochemistry of Photodynamic Sensitizers*. SPIE Volume 1065 Photodynamic Therapy: Mechanisms.
23. Huang X, Tian XJ, Yang WL, Ehrenberg B, Chen JY (2013) The conjugates of gold nanorods and chlorin e6 for enhancing the fluorescence detection and photodynamic therapy of cancers. *Phys Chem Chem Phys* 15: 15727-15733.
24. Iversena T, Skotlanda T, Sandviga T (2011) Endocytosis and intracellular transport of nanoparticles: Present knowledge and need for future studies. *Nano Today* 6: 176-185.
25. Vranic S, Boggetto N, Contremoulins V, Mornet S, Reinhardt N, et al. (2013) Deciphering the mechanisms of cellular uptake of engineered nanoparticles by accurate evaluation of internalization using imaging flow cytometry. *Part Fibre Toxicol* 10: 2.
26. Ali SM, Olivo M (2002) Bio-distribution and subcellular localization of Hypericin and its role in PDT induced apoptosis in cancer cells. *Int J Oncol* 21: 531-540.
27. Mojzisova H, Bonneau S, Vever-Bizet C, Brault D (2007) Cellular uptake and subcellular distribution of chlorin e6 as functions of pH and interactions with membranes and lipoproteins. *Biochim Biophys Acta* 1768: 2748-2756.
28. Woodburn KW, Stylli S, Hill JS, Kaye AH, Reiss JA, et al. (1992) Evaluation of tumour and tissue distribution of porphyrins for use in photodynamic therapy. *Br J Cancer* 65: 321-328.
29. Ritz R, Roser F, Radomski N, Strauss WS, Tatagiba M, et al. (2008) Subcellular colocalisation of hypericin with respect to endoplasmic reticulum and Golgi apparatus in glioblastoma cells. *Anticancer Research* 28: 2033-2038.
30. Merlin JL, Gautier H, Barberi-Heyob M, Teiten MH, Guillemin F (2003) The multidrug resistance modulator SDZ-PSC 833 potentiates the photodynamic activity of chlorin e6 independently of P-glycoprotein in multidrug resistant human breast adenocarcinoma cells. *Int J Oncol* 22: 733-739.
31. Dolmans DE, Fukumura D, Jain RK (2003) Photodynamic therapy for cancer. *Nat Rev Cancer* 3: 380-387.
32. Castano AP, Demidova TN, Hamblin MR (2004) Mechanisms in photodynamic therapy: part one-photosensitizers, photochemistry and cellular localization. *Photodiagnosis Photodyn Ther* 1: 279-293.
33. Wang XH, Peng HS, Yang L, You FT, Teng F, et al. (2014) Targetable phosphorescent oxygen nanosensors for the assessment of tumor mitochondrial dysfunction by monitoring the respiratory activity. *Angewandte Chemie International Edition English* 53: 12471-12475.
34. Feng W, Zhu X, Li F (2013) Recent advances in the optimization and functionalization of upconversion nanomaterials for in vivo bioapplications. *NPG Asia Materials* 5: e75.